Published in February 2019 issue of Journal of Molecular Structure
https://doi.org/10.1016/j.molstruc.2018.10.012

Syntheses, structures, reactivity studies and properties of anionic water rich bivalent metal phthalates

Rita N. Jyai and Bikshandarkoil R. Srinivasan*
Department of Chemistry, Goa University, Goa 403206, India
Email: srini@unigoa.ac.in

Dedicated to Prof. Dr. Wolfgang Bensch on the occasion of his 65th birthday

ABSTRACT

The syntheses and crystal structures of three anionic water rich phthalates charge balanced by piperazinediium $(pipH_2)^{2+}$ viz. $(pipH_2)[M(H_2O)_4(pht)_2]\cdot 8H_2O$ [M= Ni (**1**), Co (**2**) and Cu(**3**)] (pht = phthalate) are reported. Reaction of **1-3** with imidazole (im) results in the formation of $[M(im)_6](pht)\cdot H_2O$ [M= Ni (**4**) and Co (**5**)] and $[Cu_2(H_2O)(im)_4(pht)_2]\cdot H_2O$ (**6**) respectively. Compounds **1-6** have been characterised by spectral, thermal, electrochemical and magnetic studies and their structures determined. The phthalate ligand displays a monodentate binding mode in the bis(phthalato) compounds **1-3**. The centroid to centroid distance (Cg···Cg) between the adjacent phthalate rings in **1-3** is ~4.0 Å. In the hexaimidazole compounds **4** and **5** phthalate functions as a charge balancing dianion. The H-bonding interactions among lattice water molecules lead to the formation of a water dodecamer cluster in **1-3** with R6 water motif which further extends into a staircase pattern with T4(2)6(2) extended motif. The intra- and intermolecular H-bonding via C-H···O, N-H···O, O-H···N and O-H···O interactions results in an intricate supramolecular architecture. Thermal studies of **1-3** reveal interesting dehydration and rehydration characteristics. Compounds **1** and **2** undergo crystalline-amorphous-crystalline transformation during de- and rehydration.

Keywords: water rich; metal phthalate; piperazinediium; water dodecamer; H-bonding; crystalline-amorphous-crystalline transformation.

*For correspondence

Published in February 2019 issue of Journal of Molecular Structure
https://doi.org/10.1016/j.molstruc.2018.10.012

Introduction

Metal compounds based on benzene dicarboxylic acid have been extensively studied in the past two decades for their structural features and varied properties [1]. Since, the pioneering work by the Yaghi group of employing terephthalic acid or 1,4-benzene dicarboxylic acid (BDC) containing two carboxyl groups *trans* to each other for the construction of a highly porous metal organic framework system namely MOF-5 having composition $[Zn_4O(BDC)_3(DMF)_8(C_6H_5Cl)]$ [2], the study of metal dicarboxylates has been an active area of research. Although all three isomeric aromatic dicarboxylic acids viz. terephthalic, isophthalic and phthalic acid contain two carboxylic acid (-COOH) groups available for metal binding, which are placed on a rigid aromatic ring, the relative positioning of these carboxyl groups with respect to each other makes them distinct. Extended structures are obtained with the three isomeric dicarboxylic acids. In the case of terephthalic acid, the ligand functions as a linear bridge while binding of isophthalic acid leads to zig-zag chains. The ortho isomer viz. phthalic acid ($phtH_2$) gives rise to extended structures which can be one-dimensional (1-D) or 2-D or 3-D.

A large number of structurally characterised metal phthalate compounds which exhibit diverse phthalate binding modes are listed in the Cambridge Structural Database (CSD) [3]. Recently we reported on the synthesis and structure of $(pipH)_2[Zn(pht)_2]\cdot H_2O$ (pht = phthalate) [4] by employing the cyclic diamine piperazine (pip) as a structure directing agent. This diamine has also been used by other groups for compound synthesis [5-6]. The anionic bis(phthalate) of Zn^{2+} viz. $(pipH)_2[Zn(pht)_2]\cdot H_2O$ exhibits a one-dimensional (1-D) ladder coordination polymer structure and could also be obtained from a monomeric zinc hydrogen phthalate dihydrate $[Zn(H_2O)_2(phtH)_2]$. An analysis of the reported structures of the phthalates of Ni(II), Co(II) and Cu(II) reveals that these compounds [3, 7-37] can be classified under three categories namely anionic, cationic and neutral (Scheme S1). Very few examples of anionic phthalates having metal to phthalate ratio of 1:2 are reported so far (Table S1). In view of this, we have extended our work on zinc to a few divalent *d* metal ions and synthesised the following bis(phthalato) compounds by employing piperazinediium $(pipH_2)^{2+}$ as a charge balancing counter cation: $(pipH_2)[M(H_2O)_4(pht)_2]\cdot 8H_2O$ [M= Ni (**1**), Co (**2**) and Cu (**3**)] and $[(pipH_2)Cu(pht)_2]$ **3a**. The reaction of **1**, **2** and **3** with imidazole (im) afforded

Published in February 2019 issue of Journal of Molecular Structure
https://doi.org/10.1016/j.molstruc.2018.10.012

$[M(im)_6](pht)\cdot H_2O$ (M= Ni (**4**), Co (**5**)); $[Co(H_2O)_2(im)_3(pht)]$ **5a** and $[Cu_2(H_2O)(im)_4(pht)_2]\cdot H_2O$ **6** of which **4** and **6** were already reported by a different synthetic procedure [38, 39]. The syntheses, spectral characterization, crystal structures, electrochemical and magnetic properties of **1**-**6** are described in this report.

Experimental section

Materials and methods

All the chemicals used in this study were of reagent grade and were used as received without any further purification. Infrared (IR) spectra of the solid samples diluted with KBr were recorded on a Shimadzu (IR Prestige-21) FT-IR spectrometer from 4000-400 cm^{-1} at a resolution of 4 cm^{-1}. Raman spectra were recorded using 785 nm laser radiation for excitation on an Agiltron PeakSeeker Pro Raman instrument. UV-Visible spectra were recorded using a Shimadzu UV-2450 double beam spectrophotometer in water using matched quartz cells. Diffuse-reflectance spectra were recorded in the same instrument using $BaSO_4$ as reference (100% reflectance). Absorption data were calculated from the reflectance data using the Kubelka-Munk function ($a/S = (1-R)^2/2R$, where a is the absorption coefficient, R the reflectance, and S the Scattering coefficient. Isothermal weight loss studies were performed in a temperature controlled electric furnace. Elemental analysis (C, H and N) was performed on a Elemental vario Micro cube CHNS analyser. TG-DTA study was performed in flowing air in Al_2O_3 crucibles at heating rate of 10 K min^{-1} using a STA-409 PC simultaneous thermal analyser from Netzsch. X-ray powder pattern were recorded on a Rigaku Miniflex II powder diffractometer using Cu-K_α radiation with Ni filter. ^{1}H NMR spectra were recorded (in DMSO-d_6) using a Bruker 400 MHz (Avance) FT-NMR spectrometer. The ESR spectrum of powdered solid sample was recorded in a JOEL JES-FA200 instrument using 9.451 GHz radiation. Conductivity measurements were performed at room temperature using a Digital conductivity meter (LT-16) from Labtronics equipped with a standard conductometric cell composed of two platinum black electrodes. Cyclic voltammetry was performed in Electrochemical Workstation-CH Instrument (Inc. CH16107), by using platinum as working electrode, platinum wire as counter electrode and saturated calomel electrode (SCE) as the reference. The redox properties of the aqueous solutions of **1**, **2** and **3** were

Published in February 2019 issue of Journal of Molecular Structure
https://doi.org/10.1016/j.molstruc.2018.10.012

studied using 0.1 M KCl solution as supporting electrolyte at varying scan rates. Magnetic properties were studied as a function of temperature using a Versa Lab model vibrating sample magnetometer from Quantum Design.

*Synthesis of $(pipH_2)[M(H_2O)_4(pht)_2]\cdot 8H_2O$ (M= Ni (**1**), Co (**2**), Cu (**3**)) and $[(pipH_2)Cu(pht)_2]$ (**3a**)*

Aqueous solutions of potassium hydrogen phthalate (0.408 g, 2 mmol), pip (0.086 g, 1 mmol) and nickel chloride hexahydrate (0.237 g, 1 mmol) were mixed together to obtain a clear solution. The reaction mixture (pH = 7) was heated on a water bath to reduce the volume to 15 mL and was kept undisturbed for crystallization at room temperature. Green crystals which separated after 24 h were isolated by filtration, washed with ice cold water followed by methanol and dried in air to yield 0.622 g (90 %) of $(pipH_2)[Ni(pht)_2(H_2O)_4]\cdot 8H_2O$ **1**. Use of $[Co(H_2O)_6]Cl_2$ (0.238 g, 1 mmol) instead of $[Ni(H_2O)_6]Cl_2$ in the above reaction yielded 0.636 g (92 %) of pink crystals of **2** while use of $CuCl_2\cdot 2H_2O$ (0.170 g, 1 mmol) resulted in the formation of blue crystals of **3 (**0.418 g, 60 %) along with some green crystals of **3a**.

Anal. Calcd for $C_{20}H_{44}N_2O_{20}Ni$ (**1**): C, 34.74; N, 4.05; H, 6.43. Found: C, 34.79; N, 4.07; H, 6.38 %. IR (KBr, cm^{-1}): 3588-2506(br), 1549(s), 1414(s), 1394(s), 956(w), 818(w), 654(w). Raman (cm^{-1}): 3057(w), 1546(s), 1397(s), 1160(s), 810(s), 652(s). UV-Vis (nm): 278 (ε = 1760 mol^{-1} L cm^{-1}), 395. ^{1}H NMR (DMSO-d_6, δ from TMS): 8.171 (s, 4H), 7.496 (s, 4H), 2.884 (m, 8H). DTA (°C): 90 (endo), 320 (exo), 400 (exo). Molar conductivity (Λ_m, S cm^2 mol^{-1}) (0.01 M): 211.

Anal. Calcd for $C_{20}H_{44}N_2O_{20}Co$ (**2**): C, 34.73; N, 4.05; H, 6.43%. Found: C, 34.63; N, 4.06; H, 6.46 %. IR (KBr, cm^{-1}): 3622-2308(br), 1552(s), 1396(s), 1377(s), 1084(w), 821(w), 654(w). Raman (cm^{-1}): 3076(w), 1566(s), 1417(s), 1180(s), 1056(s), 831(s), 672(s). UV-Vis (nm): 275 (ε = 1890 mol^{-1} L cm^{-1}), 510. ^{1}H NMR (DMSO-d_6, δ from TMS): 8.6 (b, 4H), 7.7 (b, 4H). DTA (°C): 87 (endo), 119 (endo), 351 (exo), 390 (exo), 403 (exo). Molar conductivity (Λ_m, S cm^2 mol^{-1}) (0.01 M): 222.

Anal. Calcd for $C_{20}H_{44}N_2O_{20}Cu$ (**3**): C, 34.50; N, 4.02; H, 6.38%. Found: C, 34.61; N, 4.14; H, 6.28%. IR (KBr, cm^{-1}): 3514-2382(br), 1553(s), 1394(s), 1375(s), 1217(w), 1085(w), 820(w), 654(w) cm^{-1}; Raman (cm^{-1}): 3057(w), 1560(s), 1412(s), 1174(s), 1051(s), 831(s), 667(s). UV-DRS (nm): 250, 750. DTA (°C): 77 (endo), 114 (endo), 280 (exo), 324 (exo), 390 (exo).

Anal. Calcd for $C_{20}H_{20}N_2O_8Cu$ (**3a**): C, 50.04; N, 5.84; H, 4.21%. Found: C, 49.98; N, 5.80; H, 4.23 %. IR (KBr, cm^{-1}): 3601(s), 3109(br), 1562(s), 1390(s), 1365(s), 1083(w), 856(w), 831(w), 759(w), 696(w), 651(w), 516(w). UV-DRS (nm): 270, 750. DTA (°C): 270 (exo), 305 (exo), 347 (exo).

Published in February 2019 issue of Journal of Molecular Structure
https://doi.org/10.1016/j.molstruc.2018.10.012

*Synthesis of $[Ni(im)_6]pht{\cdot}H_2O$ (**4**), $[Co(im)_6]pht{\cdot}H_2O$ (**5**), $[Co(im)_3(pht)(H_2O)_2]$ (**5a**) and $[Cu_2(im)_4(pht)_2(H_2O)]{\cdot}H_2O$ (**6**)*

To an aqueous solution of **1** (0.691 g, 1 mmol) in 20 mL of distilled water, imidazole (0.273 g, 4 mmol) was added. The reaction mixture was stirred well to dissolve the N-donor ligand and left undisturbed for crystallization at room temperature. The violet crystals obtained after 7 days were isolated by filtration, washed with ice cold water and methanol and dried in air to yield 0.357 g (55 %) of $[Ni(im)_6]pht{\cdot}H_2O$ **4.** Addition of imidazole (0.273 g, 4 mmol) into an aqueous solution of **2** results in orange crystals of **5** (0.261 g, 40 %) and pink **5a** (0.191 g, 30 %), whereas the reaction of imidazole (0.136 g, 2 mmol) with **3** resulted in blue crystals of **6** (0.458 g, 60 %).

Anal. Calcd for $C_{26}H_{30}N_{12}O_5Ni$ (**4**): C, 48.09; N, 25.89; H, 4.67 %. Found: C, 48.11; N, 25.95; H, 4.63 %. IR (KBr, cm^{-1}): 3438-2630(br), 1554(s), 1379(s), 1322(w), 1250(w), 1144(w), 1072(w), 935(w), 823(w), 752(w), 665(w), 621(w), 426(w). Raman (cm^{-1}): 1597(w), 1413(w), 1328(w), 1254(s), 1160(s), 1041(w), 818(w). UV-DRS (nm): 209, 276, 390. DTA(°C): 140 (endo), 200 (endo), 395 (exo).

Anal. Calcd for $C_{26}H_{30}N_{12}O_5Co$ (**5**): C, 48.07; N, 25.88; H, 4.66 %. Found: C, 48.17; N, 25.92; H, 4.57 %. IR (KBr, cm^{-1}): 3630-2714(br), 1566(s), 1413(s), 1087(w), 752(w), 652(w), 494(w). Raman (cm^{-1}): 3143(w), 1453(w), 1320(w), 1253(s), 1148(s), 1095(w), 821(w). UV-DRS (nm): 239, 273, 494. DTA(°C): 148 (endo), 216 (endo), 415 (exo).

Anal. Calcd for $C_{17}H_{20}N_6O_6Co$ (**5a**): C, 44.06; N, 18.14; H, 4.36 %. Found: C, 44.15; N, 18.01; H, 4.5 %. IR (KBr, cm^{-1}): 3464-2623(br), 1578(s), 1493(s), 1329(s), 1255(w), 1165(w), 1070(w), 943(w), 817(w), 754(w), 698(w), 659(w), 619(w), 446(w). Raman (cm^{-1}): 1600(s), 1492(s), 1412(s), 1327(s), 1254(s), 1162(w), 1101(w), 1041(w), 818(w). UV-DRS (nm): 256, 496. DTA(°C): 129 (endo), 210 (endo), 263 (endo), 421 (exo).

Anal. Calcd for $C_{28}H_{28}N_8O_{10}Cu_2$ (**6**): C, 44.03; N, 14.67; H, 3.70 %. Found: C, 44.08; N, 14.66; H, 3.75 %. IR (KBr, cm^{-1}): 3390-2756(br), 1552(s), 1379(s), 1265(w), 1145(w), 1074(s), 954(w), 862(w), 750(w), 660(w), 462(w). Raman (cm^{-1}): 1549(s), 1362(s), 1276(s), 1205(s), 1110(s), 992(w), 770(w). UV-DRS (nm): 258, 725. DTA(°C): 148 (endo), 241 (exo), 394 (exo), 427 (exo).

Crystallography

Intensity data for **1-6** were collected at room temperature on a Bruker Smart Apex CCD diffractometer with graphite monochromated MoK_α radiation (λ=0.71073Å). The data integration and reduction were carried out using SAINT-PLUS software [40]. The structures were solved by direct methods using SHELXS-97 and refinement was done against F^2 using SHELXL-2014 [41]. All non-hydrogen atoms were refined anisotropically. All hydrogen atoms attached to the aromatic ring were introduced in calculated positions and included in the refinement riding on their respective parent C atoms. The H atoms attached to the lattice water molecules were fixed on their idealized position with

Published in February 2019 issue of Journal of Molecular Structure
https://doi.org/10.1016/j.molstruc.2018.10.012

the aid of DFIX command. The technical details of data acquisition and selected crystal refinement results for **1**-**6** are summarised in Table 1.

Results and Discussion

Synthetic aspects, spectral studies

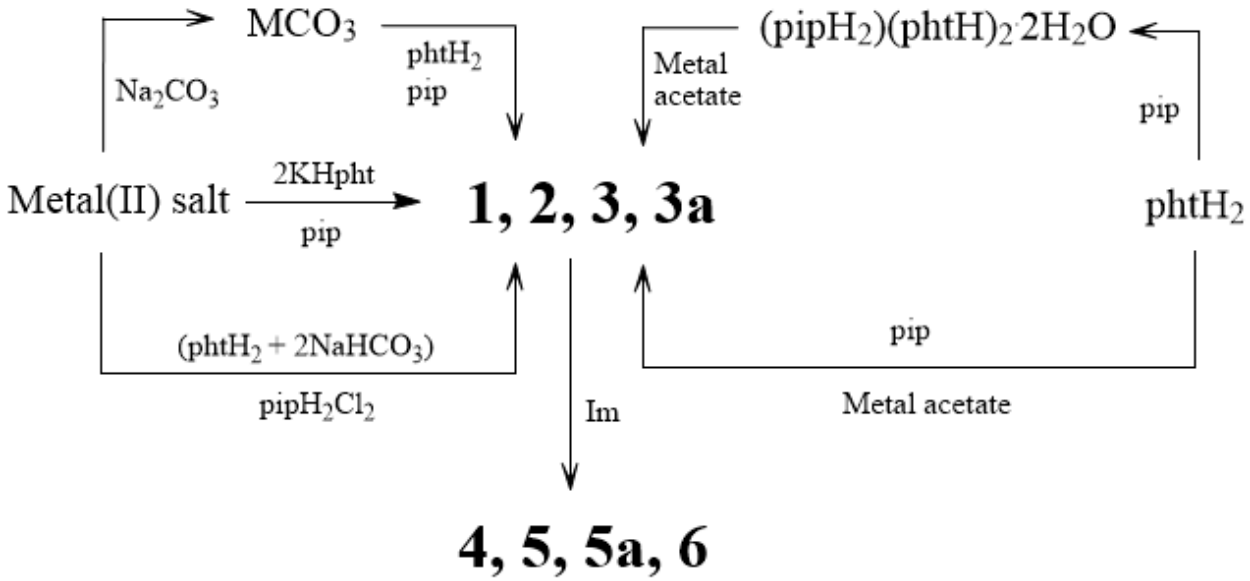

M = Ni (**1**, **4**); Co (**2**, **5**, **5a**) and Cu (**3**, **3a**, **6**)

SCHEME 1 –Synthesis of **1**, **2**, **3**, **3a**, **4**, **5**, **5a** and **6**

An aqueous reaction of potassium hydrogen phthalate (KHpht) with a Ni(II) salt in the presence of the cyclic diamine piperazine (pip) results in the formation of **1** in good yields (Scheme 1). The formation of only green crystals of **1** (Fig. S1) from the above reaction mixture using any Ni source clearly indicates that the anion (Cl^- / SO_4^{2-} / NO_3^-) has no effect on product formation and a bis(phthalato) compound charge balanced by $(pipH_2)^{2+}$ is the preferred product. The facile formation of **1** is further revealed by a single pot reaction of $Ni(OAc)_2{\cdot}2H_2O$ (OAc = acetate), phthalic acid ($phtH_2$) and pip in 1:2:1 mole ratio in aqueous medium or by an aqueous reaction of the known compound $(pipH_2)(phtH)_2{\cdot}2H_2O$ [42] with $Ni(OAc)_2{\cdot}4H_2O$ at room temperature. Alternatively, an acid-base reaction of freshly precipitated $NiCO_3$ obtained from $NiCl_2{\cdot}6H_2O$ and Na_2CO_3 with $phtH_2$ followed by addition of pip resulted in **1**. A reaction of $NiCl_2{\cdot}6H_2O$ with *in situ* generated disodium salt of $phtH_2$ and pip was used as yet another method for the synthesis of **1** (Scheme 1). The use of Co(II)

Published in February 2019 issue of Journal of Molecular Structure
https://doi.org/10.1016/j.molstruc.2018.10.012

and Cu(II) salts instead of Ni(II) salt in the above reactions resulted in pink crystals of **2** and blue crystals of **3** (Scheme 1) respectively. The facile formation of **1**-**3** under a variety of conditions reveals that when bivalent metal ions, phthalate dianion and piperazinediium cation are present in an aqueous solution, the constituents self assemble to form tetraaqua octahydrates as the major product. In the case of copper, in addition to **3**, green crystals of **3a** (Fig. S1) which lose their lustre on removal from the reaction mixture are obtained in low yield. With a view to substitute the terminal aqua ligands in **1**-**3** by N-donors, a ligand exchange reaction was performed by reaction of **1**-**3** with imidazole in a 1:4 mole ratio. Contrary to our expectations these reactions did not give rise to any anionic bis(phthalates) but resulted in the formation of 1:1 phthalates devoid of any organic cation viz. blue crystals of **4** and orange crystals of **5** with a metal:im stoichiometry of 1:6, and blue crystals of **6** showing a 1:2 Cu:im composition (Scheme 1). In the literature, compounds **4** and **6** have been prepared without use of piperazine [38, 39]. The reaction of imidazole with **2** afforded pink crystals of **5a** in addition to **5** which exhibits a Co:im ratio of 1:3 (Fig. S1). Compounds **3a** and **5a** could be easily separated manually from the reaction mixture and were formulated based on analytical data. The composition of all compounds was initially arrived at based on elemental analysis, mass loss studies and metal oxide formed on pyrolysis and unambiguously confirmed by single crystal X-ray studies for **1**-**6**.

The IR spectra of all compounds studied in this work exhibit several signals in the mid-IR region indicating the presence of organic moieties (Fig. S2). A characteristic feature of the infrared spectra of the water rich compounds **1**-**3**, is the observation of a very similar strong and broad signal in the 3500-2500 cm^{-1} region which can be assigned for the –OH stretching vibrations as well as the H-bonding interactions (*vide infra*) of the water molecules. The absence of a signal in the region 1680-1710 cm^{-1} (expected for –COOH) clearly indicates the formation of the fully deprotonated phthalate dianion in all these compounds. In the IR spectrum of **1**, an intense band at 1549 cm^{-1} (1552 in **2**; 1553 in **3**; 1562 in **3a**; 1558 in **4**; 1566 in **5**; 1578 in **5a**; 1552 in **6**) can be assigned for the asymmetric stretching vibration of the carboxylate group (υ_{asym}) and the bands observed at 1414 and 1394 cm^{-1} (1396 and 1377 in **2**; 1394 and 1375 in **3**; 1390 and 1365 in **3a**; 1379 in **4**; 1413 in **5**; 1406 in **5a**; 1379 in **6**) for symmetric stretching vibration (υ_{sym}). The IR stretching vibrations expected for the υ_{N-H} vibration of

Published in February 2019 issue of Journal of Molecular Structure
https://doi.org/10.1016/j.molstruc.2018.10.012

the imidazole ligand group in 3500 – 3350 cm^{-1} region is masked in the broad –OH band in compounds **4-6**. Interestingly compound **1** exhibits two signals at 1546 and 1397 cm^{-1} in its Raman spectrum (1566 and 1417 in **2**; 1560 and 1412 in **3**; 1597 and 1413 in **4**; 1453 and 1320 in **5;** 1600 and 1412 in **5a**; 1549 and 1362 in **6**) (Fig. S2) with the latter being more intense and assignable for the asymmetric (υ_{asym}) and symmetric stretching vibrations (υ_{sym}) of the carboxylate group respectively. The UV-Vis spectra of all compounds are characteristic of an absorption at ~275 nm. The optical spectra (Fig. S3) in water and in solid-state (Fig. S4) of **1-2** exhibit a band around 275 nm that can be assigned for the intra-ligand charge transfer of the aromatic phthalate. The band at 395 nm for **1** (510 nm for **2**) can be attributed to the *d-d* transition of the respective bivalent metal ions. Due to solubility issues compounds **3**, **3a**, **4**, **5**, **5a** and **6** were studied by diffuse reflectance spectra (DRS). Compound **3** (**3a**) (Fig. S3) exhibits a band at 252 (270 nm) for intra-ligand charge transfer of aromatic phthalate group and a broad band above 750 nm. The DRS of **4** (Fig. S3) exhibits bands at 209 and 276 (239 and 273 nm for **5**; 256 for **5a**; 258 for **6**) for intra-ligand charge transfer and 390 nm (494 nm for **5**; 496 for **5a**; 725 for **6**) assignable for a possible metal centered transition of the respective metal ion. The ^{1}H NMR spectrum of **1** (Fig. S5) exhibits the characteristic resonances of the aromatic protons of phthalate ligand at δ 8.17 and δ 7.50 ppm respectively in addition to a signal for -CH_2 protons of piperazine δ 2.88 ppm. From the integration of the peaks the pht:pip ratio can be inferred as 2:1. Thus the NMR experiment serves to determine the presence as well as the stoichiometry of the phthalate and piperazinediium moieties in **1**. The PMR spectrum of **2** (Fig. S5) can be similarly explained and the broad resonances can be attributed to the paramagnetic nature of Co^{2+}. In the case of **3**, no NMR signals could be obtained in the normal range. Hence, **3** was studied by ESR method. The room temperature ESR spectrum (Fig. S6) exhibits axial symmetry with $g_{||} > g_{\perp} > 2.03$ ($g_{||} = 2.3119$ and $g_{\perp} = 2.0920$), usually observed in Cu(II) ions having–square-planar geometry and with the unpaired electron localized in $d_{x^2-y^2}$ orbital giving $^{2}B_{1g}$ as ground state [43]. The powder pattern of all compounds exhibit sharp Bragg lines indicating their crystalline nature. The minor products **3a** and **5a** exhibit differing powder patterns as compared to the water rich compound **3** and the hexaimidazole compound **5** respectively. The experimental powder pattern of the bulk sample is in very good agreement with the theoretical powder pattern calculated from the single crystal data (*vide infra*) of **1-**

Published in February 2019 issue of Journal of Molecular Structure
https://doi.org/10.1016/j.molstruc.2018.10.012

6 (Fig. S7). The results of powder pattern experiments, reproducible thermo analytical data and spectral data reveal that all the compounds can be obtained in a state of high purity.

Thermal investigations, electrochemistry and magnetic studies

Compound **1** exhibits an endothermic event with a peak in DTA at 90°C in its TG-DTA graph (Fig. S8). The TG curve shows a decrease in mass by 26.13 % equivalent to loss of 10 water molecules at 100°C and a gradual decrease by 31.83 % at 180°C equivalent to 12 water molecules (fully dehydrated compound). Above 200°C, the DTA curve shows only exothermic peaks at 320°C and 400°C, accompanied by a rapid drop in mass that can be attributed to decomposition of **1**. The residual mass of 10.93 % is in very good agreement for the formation of NiO. Compound **2** exhibits endothermic events at 87°C and 119°C in its TG-DTA graph (Fig. S8). The TG curve shows a decrease in mass by 22.28 % equivalent to loss of 8 water molecules at 100°C and a gradual decrease by 31.53 % at 180°C equivalent to 12 water molecules (fully dehydrated compound). Above 200°C, the DTA curve shows only exothermic peaks at 351°C, 390°C and 403°C with rapid mass loss due to decomposition of **2**. The residual mass of 11.5 % corresponds to Co_3O_4 as confirmed by powder pattern. Similarly, an endothermic peak in DTA at 77 and 114°C was observed for compound **3** in its TG-DTA graph (Fig. S8). Its TG curve shows a decrease in mass by 27.23 % equivalent to loss of 10 water molecules at 100°C and a gradual decrease by 30.89 % at 180°C equivalent to 12 water molecules (fully dehydrated compound). Above 200°C, the DTA curve shows only exothermic peaks at 280°C, 324°C and 390°C, followed by a rapid drop in mass due to decomposition of **3**. The residual mass of 11.35 % is in accordance with the formation of CuO. The TG curve of **3a** (Fig. S8) shows no weight loss till 240°C indicating the anhydrous nature of the compound. Above 250°C, the DTA curve of **3a** shows a similar pattern to compound **3** with exothermic peaks at 270°C, 305°C and 347°C. The % residue obtained 17.13 % is in good agreement with the CuO formed on heating the compound at 600°C in the electric furnace. Compound **4** exhibits an endothermic event at 140°C in its TG-DTA graph (Fig. S8). The TG curve shows a decrease in mass by 2.77 % equivalent to the loss of a single water molecule by 150°C. The DTA curve shows an endothermic and exothermic peak at 200°C and 395°C respectively, accompanied by a rapid drop in mass that can be attributed to

Published in February 2019 issue of Journal of Molecular Structure
https://doi.org/10.1016/j.molstruc.2018.10.012

decomposition of **4**. The residual mass of 11.5 % is in very good agreement for the formation of NiO. Compound **5** shows an endothermic peak at 148°C in its TG-DTA graph (Fig. S8). The TG curve shows a decrease in mass by 2.8 % equivalent to loss of one water molecule at 150°C. Above 200°C, the DTA curve shows an endothermic peak at 216°C and an exothermic peak at 415°C, accompanied by a rapid mass loss that can be attributed the decomposition of **5**. The residual mass of 12.32 % is in good agreement for the formation of Co_3O_4 further confirmed by powder pattern. The DTA curve of compound **5a** shows three endothermic peaks 129, 210, 263°C and an exothermic peak at 421°C, accompanied by a rapid mass loss in its TG-DTA graph (Fig. S8) that can be attributed the decomposition of **5a**. The residual mass of 17.25 % is in good agreement for the formation of Co_3O_4. Compound **6** exhibits an endothermic event at 150°C in its TG-DTA graph (Fig. S8). The TG curve shows a decrease in mass by 4.72 % assignable for the loss of 2 water molecules at 150°C. Above 200°C, the DTA curve shows only exothermic peaks at 241, 394 and 427°C, accompanied by a rapid drop in mass that can be attributed to decomposition of **6**. The residual mass of 21.28 % is in very good agreement for the formation of CuO. The featureless IR spectra (Fig. S9) of the residues obtained and their matching powder patterns with corresponding oxides (Fig. S9) provide evidence for the complete removal of organic moiety with oxide formation. The results of isothermal mass loss studies performed at different temperatures viz. 100°, 150°, 180°, 200° and 600°C add credence to the thermal data of the compounds.

The room temperature conductivity of aqueous solutions of **1** and **2** (Table 2) exhibit an increase in molar conductivity values with increasing dilution indicating the dissociation of both compounds in dilute solution.

Published in February 2019 issue of Journal of Molecular Structure
https://doi.org/10.1016/j.molstruc.2018.10.012

Table 2: Specific conductivity (Ƙ) and molar conductivity (Λ_m) data for **1** and **2** at room temperature

Molar concentration (M)	Specific conductivity (Ƙ) (in S cm^{-1})		Molar conductivity (Λ_m) (S cm^2 mol^{-1})	
	1	**2**	**1**	**2**
0.1	7.12	8.29	71	83
0.08	6.53	7.12	82	89
0.06	5.72	6.53	95	109
0.04	4.78	5.37	119	134
0.02	3.26	3.62	163	181
0.01	2.11	2.22	211	222
0.001	0.49	0.65	494	645

The electrochemistry of **1**-**2** was studied by cyclic voltametry at room temperature in the potential range 1 to -1 V using 0.1 M KCl aqueous solution as a supporting electrolyte (Fig. 1, Fig. S10). A pair of redox events was observed in the potential range of -0.2 to -0.9 V and -0.1 to -0.9 for **1** and **2** respectively, which can be attributed to a ligand (phthalate) centred process. The effect of varying the scan rate from 0.02 to 0.1 Vs^{-1} does not show any remarkable changes in $E_{1/2}$ excepting a slight increase in the peak-to-peak separations.

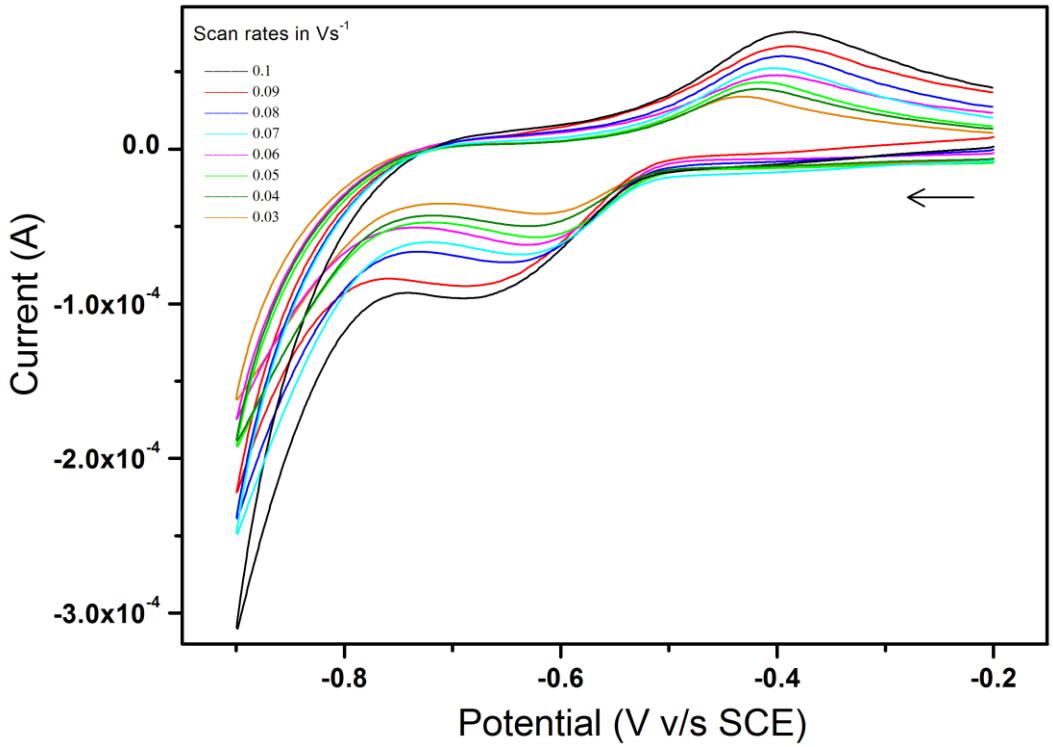

Fig. 1 - Cyclic voltammograms of **1** at different scan rates (from inner to outer) of 0.03, 0.04, 0.05, 0.06, 0.07, 0.08, 0.09 and 0.1Vs^{-1} in the potential range of -0.9 to -0.2V in 0.1M aqueous KCl solution. (For cyclic voltammogram of **2** see fig. S10)

Published in February 2019 issue of Journal of Molecular Structure
https://doi.org/10.1016/j.molstruc.2018.10.012

The temperature-dependent magnetic susceptibility of polycrystalline samples of **1**, **2**, **3**, **3a**, **5** and **5a** have been measured at an applied magnetic field of 250 Oe in the temperature range 50-300K (Fig. S11-S13). The χ_M versus T plots depict a simple paramagnetic behaviour of all indicating the absence of exchange interactions. This behaviour is in accordance with the central structures which show that the metal centres are located far apart from each other.

*Dehydration-rehydration studies of **1**, **2** and **3***

Heating of the water rich compounds **1**-**3** at 180°C results in a marked colour change from green to yellowish green (for **1**), pink to violet (for **2**), blue to dark green (for **3**) affording the completely dehydrated product. The anhydrous phase thus formed can be rehydrated to the starting materials by equilibriation of the dehydrated product over an atmosphere of water vapour in a closed dessicator for 4 days. In a typical experiment, a weighed amount (100 mg) of **1** (or **2** or **3**) was heated at 180°C in an oven for 15 minutes. The measured weight loss of 31.32 mg (31.32 %) for **1**, 31.30 mg (31.30 %) for **2** and 31.15 mg (31.15 %) for **3** was in good agreement for the loss of 12 water molecules and formation of fully dehydrated compounds. This is in agreement with the elemental analysis.

(Anhydrous **1**): Anal. (%): Found (calcd) for $NiC_{16}N_2O_9H_{12}$ (475.11): C 40.42 (40.45), H 2.57 (2.55), N 5.7 (5.9); (Anhydrous **2**): Anal. (%): Found (calcd) for $CoC_{16}N_2O_9H_{12}$ (475.35): C 40.39 (40.42), H 2.58 (2.54), N 5.85 (5.89); (Anhydrous **3**): Anal. (%): Found (calcd) for $CuC_{16}N_2O_9H_{12}$ (479.97): C 40.01 (40.04), H 2.55 (2.53), N 5.81 (5.84).

The IR spectra and powder pattern of **1**-**3** heated at 100, 150 and 180°C depict stepwise removal of water molecules (Fig. 2, Fig. S14-S15). The anhydrous compound thus formed is amorphous which can be transformed to the original hydrated starting material. The regenerated materials show an increase in their mass viz. 31.32, 31.30 and 31.15 mg for **1**, **2** and **3** respectively. This gain in weight corresponds to the addition of 12 water molecules, as evidenced by identical IR spectra and powder pattern (Fig. S14-S15) with those of the respective starting compounds. The powder pattern demonstrates an interesting crystalline-amorphous-crystalline phase transformation for **1** and **2**. Thus, compounds **1**-**3** can be considered as a molecular water reservoir as the lattice water molecules can be completely removed and put back in the crystal host to regain its original structure. Interestingly, compound **3a** when kept in an aqueous atmosphere in a dessicator absorbs moisture and gets hydrated

Published in February 2019 issue of Journal of Molecular Structure
https://doi.org/10.1016/j.molstruc.2018.10.012

to **3** over a period of 5 days (Fig. S16). However this hydrated compound **3** from **3a** on dehydration doesn't revert to **3a**.

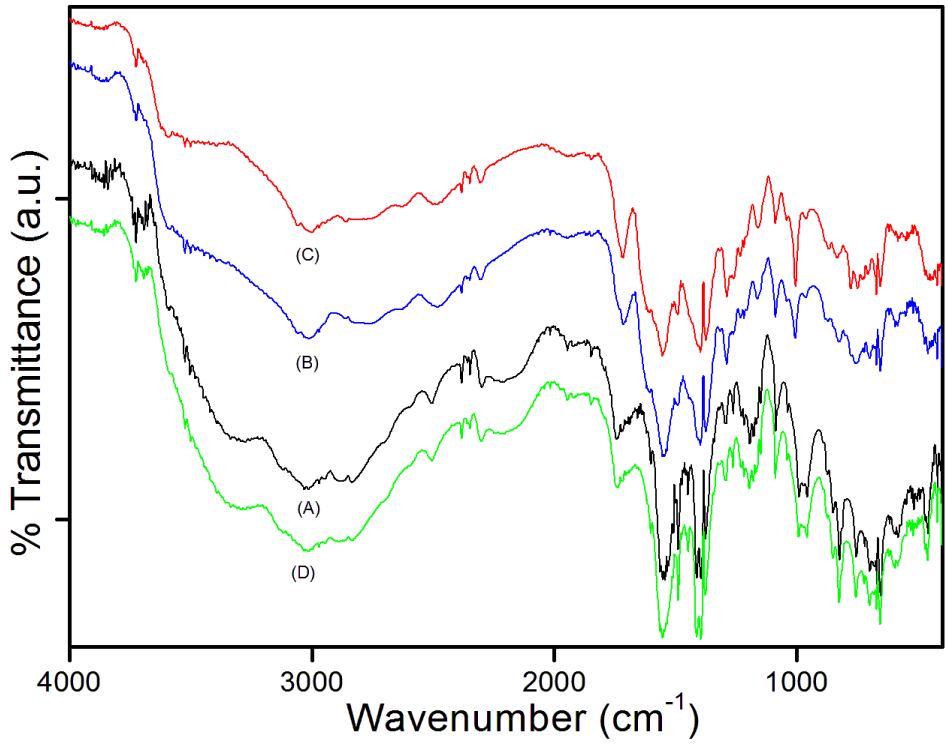

Fig. 2 – IR spectrum of **1** dehydrated at different temperatures (A) Starting compound, (B) at 100°, (C) at 180° and (D) Rehydrated compound. (For IR spectra of **2** and **3** dehydrated at different temperatures see fig. S14)

Description of crystal structures

The anionic water rich bis(phthalato) compounds **1-3** crystallise in the centrosymmetric triclinic *Pī* space group. The structures of all three compounds are based on a metal bis(phthalato) anionic unit with two independent monodentate pht^{2-} ligands disposed *trans* to each other and charge balanced by an organic cation $(pipH_2)^{2+}$. The geometric parameters of the phthalate ligands are in the normal range and are in agreement with reported data (Table S2). The unique organic cations are diprotonated and adopt a chair conformation with their geometric parameters in normal range and are in very good agreement with reported data [44, 45 Table S3]. The central metal ion viz. Ni(II) in **1** and Co(II) in **2** Cu(II) in **3** exhibit hexacoordination forming a distorted $\{MO_6\}$ octahedron. Although compounds **1-3** have similar anionic units, they differ from each other in terms of the number of unique metal ions present in the crystal structure. Compound **1** contains an unique Ni(II) ion situated in a general

Published in February 2019 issue of Journal of Molecular Structure
https://doi.org/10.1016/j.molstruc.2018.10.012

position while three independent Co(II) ions one of which (Co3) is situated on an inversion centre are present in **2**. Compound **3** contains two unique metal ions one of which (Cu2) is located on an inversion centre (Fig. 3-4, Fig. S17-S18).

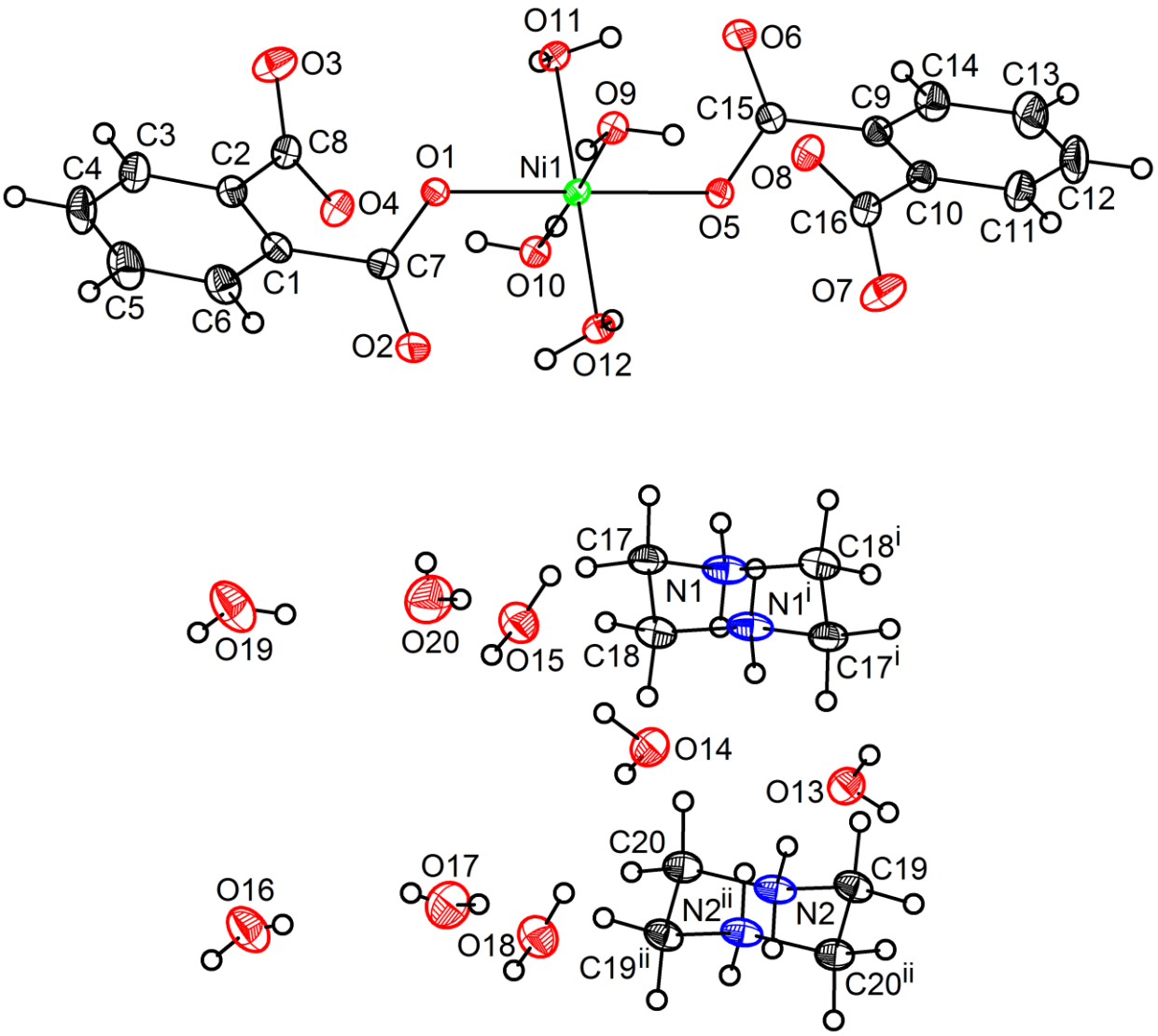

Fig. 3 – The crystal structure of $(pipH_2)[Ni(H_2O)_4(pht)_2]\cdot 8H_2O$ (**1**) showing the atom labelling scheme and the coordination sphere of Ni(II) in **1**. Displacement ellipsoids are drawn at the 50% probability level excepting for the H atoms, which are shown as circles of arbitrary radius. Symmetry code: i) 1-x, 1-y, 1-z; ii) 2-x,-y, 1-z. (for crystal structure of **2** refer fig. S17)

Published in February 2019 issue of Journal of Molecular Structure
https://doi.org/10.1016/j.molstruc.2018.10.012

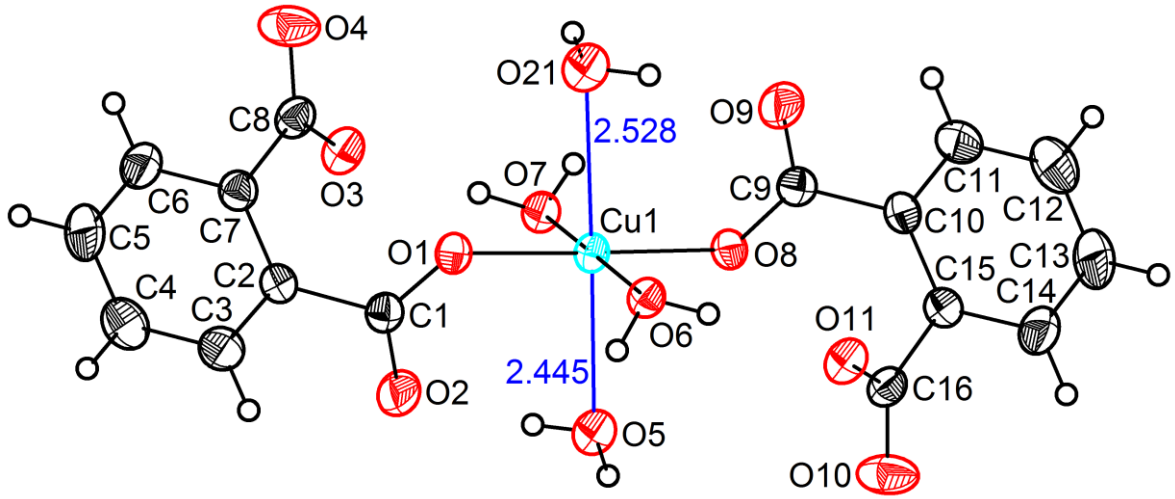

Fig. 4 – The anionic unit present in the crystal structure of $(pipH_2)[Cu(H_2O)_4(pht)_2]\cdot 8H_2O$ (**3**) showing the atom labelling scheme and the distorted octahedral coordination around Cu(II). Displacement ellipsoids are drawn at the 50% probability level excepting for the H atoms, which are shown as circles of arbitrary radius. Symmetry code: i) -x, 1-y, 1-z; ii) -x, 1-y, -z. The other anionic unit, cation and lattice water molecules are shown in fig. S18.

Despite the presence of more than one unique metal in **2** and **3**, all metal centres exhibit the same hexacoordination viz. four terminal aqua ligands and two monodentate phthalates, due to the presence of five crystallographically unique phthalate ligands in **2** and three independent phthalates in **3**. The M-O bond distances range from 2.0402(11) to 2.1070(11) Å (Ni-O) and 2.0697(13) to 2.1509(13) Å (Co-O). The O-M-O angles vary between 86.36(5) to 94.65(5)° (cis angles) and 177.08(4) to 179.29(4)° (trans angles) in **1**, 85.00(5) to 95.81(5)° (cis angles) and 176.58(5) to 179.43(5)° (trans angles) in **2** indicating a slightly distorted $\{MO_6\}$ octahedra (Table S4). Four Cu-O bond distances in **3** range from 1.941(7) to 1.988(8) Å (Cu-O) while the O-Cu-O cis angles vary between 88.2(3) to 92.5(3)° and trans angles from 177.7(3) to 178.8(3)°. In addition, two longer Cu-O(H_2O) distances at 2.445(2) and 2.528(5) Å in Cu1 are observed indicating a Jahn-Teller distorted $\{CuO_6\}$ octahedron (Table S4). The second unique Cu2 in **3** exhibits a similar distorted $\{CuO_6\}$ octahedron.

It is interesting to note that the phthalate anion in **1**-**3** functions as a monodentate ligand and not as a bridging ligand which is often observed in many other bivalent metal phthalates. An analysis of the crystal structures of several phthalates (Table S1) reveals that i) majority of the compounds crystallizes in centrosymmetric space group and ii) in compounds with less number of coordinated

Published in February 2019 issue of Journal of Molecular Structure
https://doi.org/10.1016/j.molstruc.2018.10.012

water molecules the phthalate ligand adopts a bridging binding mode. Hence, the observed monodentate ligation of $(pht)^{2-}$ can be correlated to the degree of hydration of these compounds. All these compounds contain four terminal aqua ligands and eight lattice water molecules.

It is interesting to note that compounds **1-3** are rare examples of metal phthalates containing a dozen water molecules per metal and hence we have used the terminology 'water rich' to designate these compounds. In the Ni(II) series only one compound viz. $[Ni(pht)(Bpybc)(H_2O)_4]\cdot 9H_2O$ (Bpybc= 1,1'-bis(4-carboxylatobenzyl)-4,4'-bipyridinium) [46] is reported so far containing high metal: H_2O ratio of 1:13 (Scheme S2). Since the hydrogens of the lattice waters were not located an analysis of the water architecture was not reported. An analysis of the crystal structures of **1-3** reveals that the coordinated and lattice water molecules exhibit several intra- and intermolecular H-bonding interactions (Table S5; Fig. S19-S21) due to the presence of a dozen water molecules, resulting in an intricate 3-D supramolecular architecture. The intramolecular H-bonding among the lattice water molecules in **1-3** results in the formation of a water dodecamer cluster (R6 water motif) which extends on both sides forming a tetramer with the next cyclic hexameric unit resulting in an alternate arrangement of edge-shared hexameric and tetrameric units of water dodecamer having T4(2)6(2) extended motif. Based on the nomenclature of various types of water clusters, extended water motifs reported by Infantes *et al* [47] the water cluster in **1-3** is designated as R6 and the extended motif is termed as T4(2)6(2). The observed average O···O distance in water dodecamer cluster in **1-3** is 2.824 Å, which is shorter than those observed in liquid water (2.854 Å) and thus comparable to those in the ice phase (2.77 - 2.84 Å) [48-50]. In **1**, a water dodecamer cluster of type 'A' (Fig. 5) is formed by O15, O16, O17, O18, O19 and O20 with six water molecules O13, O14, O16, O17, O19 and O20 bonded to every corner. The cyclic hexamer is non-planar and extends on one side via O16 and O17 and on the opposite side via O19 and O20 forming a tetramer with the next identical cyclic hexameric unit 'A'. This results in an alternate arrangement of edge-shared hexameric and tetrameric units resulting in a H-bonded sequence '-A-A-A-' of water dodecamer having T4(2)6(2) extended motif (Fig. 5). Due to the non-planar nature of the hexameric unit, the extended water cluster resembles a staircase pattern when viewed along *c-axis* (Fig. S22). Due to the presence of three unique

Published in February 2019 issue of Journal of Molecular Structure
https://doi.org/10.1016/j.molstruc.2018.10.012

bis(phthalato) Co(II) in **2**, three types of water dodecamer clusters are formed viz. 'A', 'B' and 'C' with 'A' located on an inversion centre (Fig. S23). The water dodecamer cluster 'A' is formed using O34, O35, O36, O37, O38 and O50; cluster 'B' via H-bonding between 031, O32, O33, O34, O35, O37, O38, O39, O42, O43, O44, and O49 while cluster 'C' is formed of O33, O40, O41, O43, O44, O45, O46, O47, O48 and O49. Water cluster 'A' extends on either side via O34 and O35; cluster 'B' using O37 and O38 on one side and on the other side via O44 and O49 whereas cluster 'C' extends by means of O33 and O43 on one side and O45 and O46 on the other side in the order '-B-A-B-C-C-B-A-B-' (Fig. S23). The extension of these water dodecamer units again results in a staircase pattern as in **1** when viewed along *b-axis* (Fig. S23). The two types of water dodecamer clusters namely 'A' and 'B' in **3** can be explained due to the presence of the two unique bis(phthalato) Cu(II) units, with 'A' located on an inversion centre (Fig. S24). The water dodecamer cluster 'A' is made up of O22, O23, O24, O25, O28 and O29 while cluster 'B' is formed using O17, O18, O19, O20, O22, O23, O24, O25, O26 and O27. Water cluster 'A' extends on either side using O24 and O25 whereas cluster 'B' extends by means of O18 and O19 on one side and O22 and O23 on the other side in the sequence '-A-B-B-A-B-B-A-' resembling a staircase structure motif as in **1** and **2** when viewed along *b-axis* (Fig. S24).

Further, the unique cations serve as crosslinks between two successive extended water motifs via N-H···O interactions forming a two dimensional (2-D) sheet. In **1**, the two water molecules O13 and O14 attached to the cyclic hexamer but not involved in its extension are H-bonded to the nitrogen atoms N1 and N2 of two unique organic cations pipN1 and pipN2 interlinking the two cations via N1···O13···N2 and N1···O14···N2 linkages. The two unique cations pipN1 and pipN2 serve as crosslinks between two successive water staircases forming a 2-D sheet in the crystallographic *ac* plane (Fig. 5). A similar type of sheet structure is observed in **2** and **3** (Fig. S25-S26). The H-bonding amongst cation, anion and water cluster **1**-**3** leads to a cage architecture of the metal centres with the longest M···M distance of the order of 12 Å (Fig. 6, Fig. S27-S28). Such long M···M distances can very well explain the paramagnetic behaviour of the water rich mononuclear compounds **1**-**3**.

Published in February 2019 issue of Journal of Molecular Structure
https://doi.org/10.1016/j.molstruc.2018.10.012

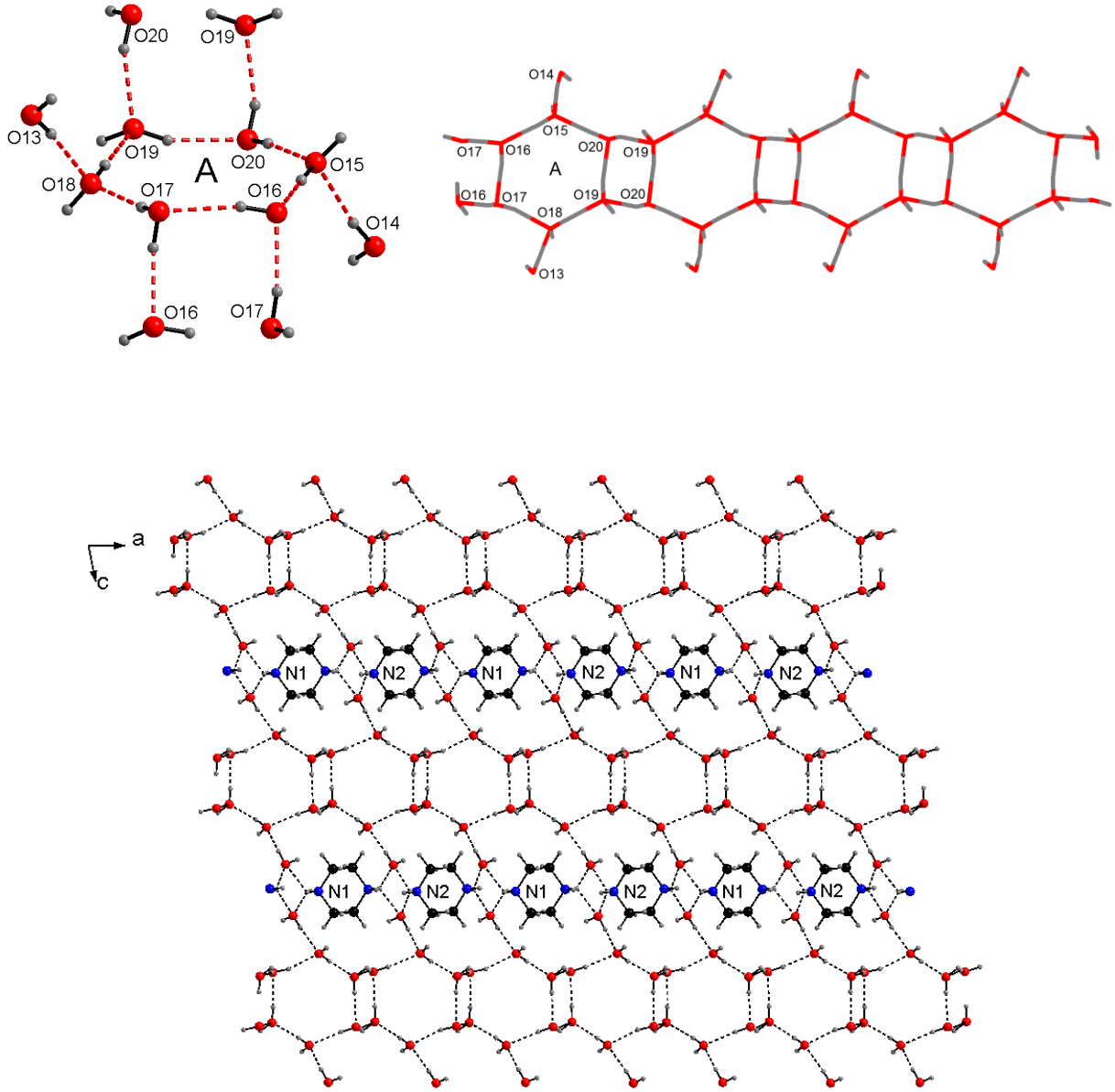

Fig. 5 - A water dodecamer ‘A’ formed by H-bonding interactions among lattice water molecules (top left) extending on either side having an alternate arrangement of edge-shared hexameric and tetrameric unit in the sequence ‘-A-A-A-’ (top right). The unique piperazinediium pipN1 and pipN2 cross links two infinte water staircase via N-H···O H-bonding interaction forming a cation-water sheet in the crystallographic *ac* plane in **1** (For the water dodecamer, extended water motif and the corresponding cation-water sheet in **2** and **3** see fig. S23-S26)

Published in February 2019 issue of Journal of Molecular Structure
https://doi.org/10.1016/j.molstruc.2018.10.012

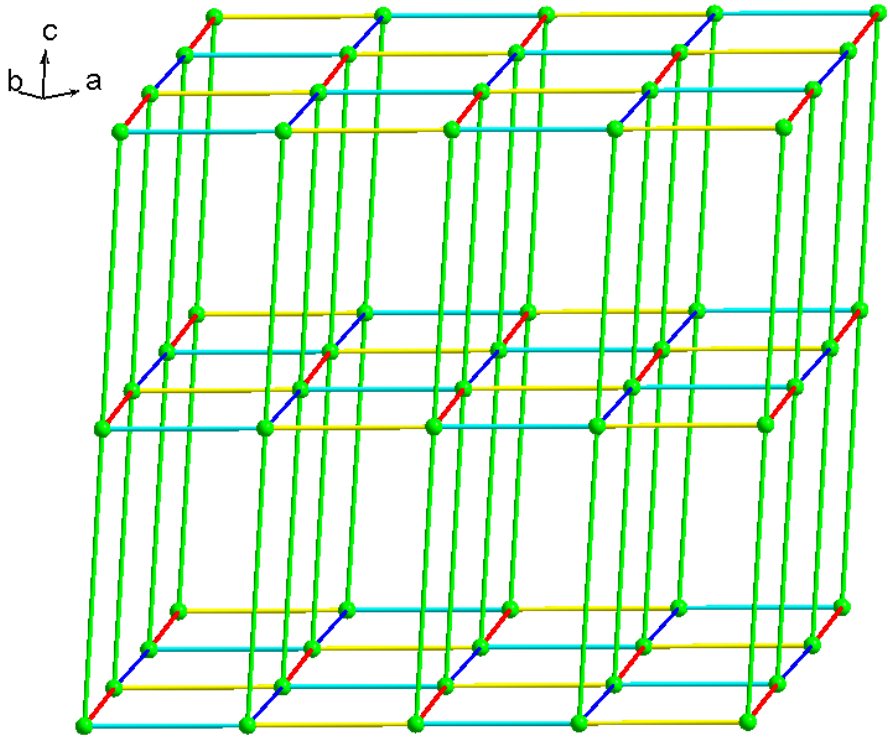

Fig. 6 – The organisation of Ni(II) centres in the crystal structure of **1** showing a 3-D cage architecture with Ni···Ni separation of 12.496 Å (Green), 8.684 Å (Red), 9.580 Å (Blue), 7.072 Å (Cyan) and 7.112 Å (Yellow) (for cage architecture in **2** and **3** see fig. S27-S28)

In addition to the H-bonding interactions described above, the water rich compounds **1**-**3** exhibit π···π stacking interactions [51]. For the analysis of short ring interactions in **1**-**3** the program Platon [52] was used and the details are listed in Table 3. In compounds **1**-**3** the ring centroid to ring centroid distances (Cg···Cg) between adjacent phthalates are found to be of the order of 4 Å. The shortest Cg···Cg distances in **1**, **2** and **3** are 4.0964, 4.0772 and 4.0876 Å respectively. As it has been reported that stacking interactions between benzene rings can exist at very long Cg···Cg (Cg = ring centroid) distances up to 7 Å [53], the observed (Cg···Cg) distances can be attributed to π···π stacking of the six membered rings. A representative π···π stacking interaction in **1** is displayed in Fig. 7.

Published in February 2019 issue of Journal of Molecular Structure
https://doi.org/10.1016/j.molstruc.2018.10.012

Table 3 - Analysis of Short Ring-Interactions with Cg-Cg Distances < 6.0 Å and β < 60.0^0

Cg(I)	Res(I)	Cg(J)	[ARU(J)]	Cg-Cg	α	B	γ	CgI_Perp	Cg J_Perp	Slippage
$(pipH_2)[Ni(H_2O)_4(pht)_2]\cdot 8H_2O$ **1**										
Cg(1)	[1] ->	Cg(1)	[2655.01]	4.0964(11)	0	26	26	3.6824(8)	3.6824(8)	1.795
Cg(2)	[1] ->	Cg(2)	[2567.01]	4.1616(12)	0	24	24	-3.8030(8)	-3.8030(8)	1.69
Where, Cg(1)= first phthalate (C1-C6) and Cg(2)= second unique phthalate (C9-C14)										
$(pipH_2)[Co(H_2O)_4(pht)_2]\cdot 8H_2O$ **2**										
Cg(1)	[1] ->	Cg(1)	[2775.01]	4.0772(13)	0	25.5	25.5	-3.6804(9)	-3.6804(9)	1.754
Cg(2)	[1] ->	Cg(3)	[1545.02]	4.1148(13)	0.55(11)	23.5	23.8	-3.7638(9)	3.7723(9)	
Cg(4)	[2] ->	Cg(5)	[1545.03]	4.1222(13)	1.78(11)	26.6	26.8	-3.6808(9)	3.6867(9)	
Where, Cg(1)= first phthalate (C2-C7), Cg(2)= second unique phthalate (C10-C15), Cg(3)= third unique phthalate (C18-C23), Cg(4)= fourth unique phthalate (C26-C31) and Cg(5)= fifth unique phthalate (C34-C39)										
$(pipH_2)[Cu(H_2O)_4(pht)_2]\cdot 8H_2O$ **3**										
Cg(1)	[1] ->	Cg(1)	[2676.01]	4.0876(14)	0	22.7	22.7	3.7706(10)	3.7707(10)	1.578
Cg(2)	[1] ->	Cg(3)	[1545.02]	4.1116(14)	1.79(11)	27	26.4	3.6815(10)	-3.6642(9)	
Where, Cg(1)= first phthalate (C2-C7), Cg(2)= second unique phthalate (C10-C15) and Cg(3)= third unique phthalate (C18-C23)										

- Cg(I) = Plane number I (= ring number in () above)
- Alpha = Dihedral Angle between Planes I and J (Deg)
- Beta = Angle Cg(I)-->Cg(J) or Cg(I)-->Me vector and normal to plane I (Deg)
- Gamma = Angle Cg(I)-->Cg(J) vector and normal to plane J (Deg)
- Cg-Cg = Distance between ring Centroids (Ang.)
- CgI_Perp = Perpendicular distance of Cg(I) on ring J (Ang.)
- CgJ_Perp = Perpendicular distance of Cg(J) on ring I (Ang.)
- Slippage = Distance between Cg(I) and Perpendicular Projection of Cg(J) on Ring I (Ang.)

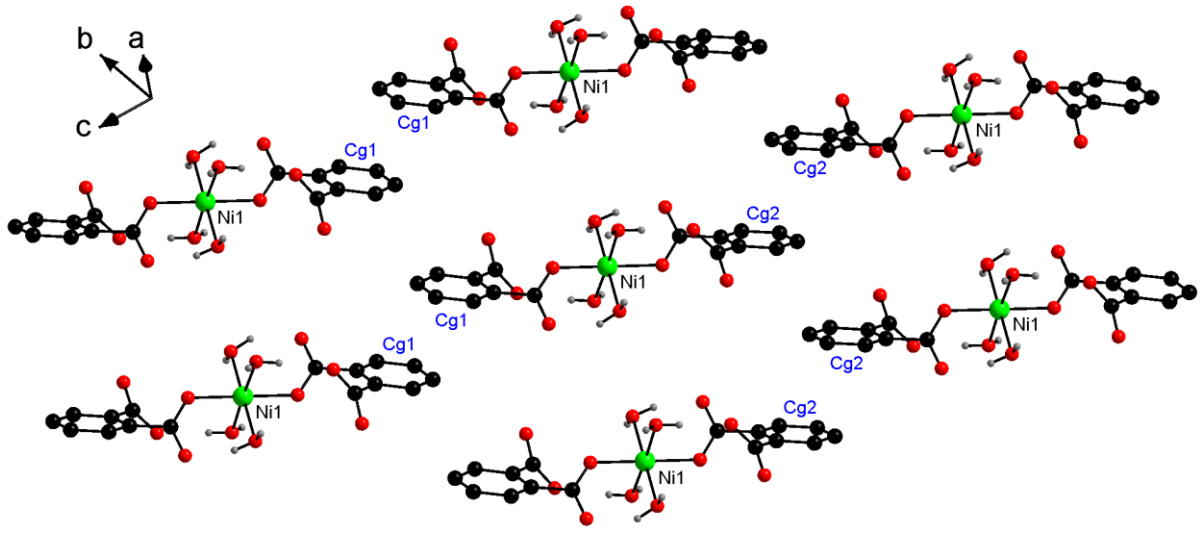

Fig. 7 – π···π stacking in **1** [Cg(1) = unique phthalate ligand and Cg(2) = second unique phthalate ligand]

Compounds **4** and **5** contain the hexaimidazole metal unit $[M(im)_6]^{2+}$ (M= Ni **4**; Co **5**) charge balanced by phthalate anion while **6** is a dinuclear copper compound containing terminal imidazole and bridging phthalate ligand. **4** and **6** are reported compounds and **5** is isostructural to **4**. Therefore, only the crystal structure of **5** is briefly discussed herein. Compound **5** crystallises in the

Published in February 2019 issue of Journal of Molecular Structure
https://doi.org/10.1016/j.molstruc.2018.10.012

centrosymmetric monoclinic $P2_1/c$ space group. The crystal structure of **5** consists of an unique Co(II) ion, six crystallographically independent imidazole ligands, an unique phthalate and a lattice water molecule, all of which are situated in general positions (Fig. 8). The central metal ion is octahedrally coordinated to six nitrogen atoms from six terminal imidazole ligands. In this case, the phthalate dianion acts as a charge balancing counter anion. The metric parameters of imidazole ligands and phthalate anion are in normal range (Table S2). The Co-N bond distances range from 2.153(2) to 2.195(2) Å. The cis N-Co-N angles vary between 87.74(9) to 92.52(9)° and the trans angles range from 177.01(8) to 177.93(9)° indicating a distorted $\{CoN_6\}$ octahedron (Table S4).

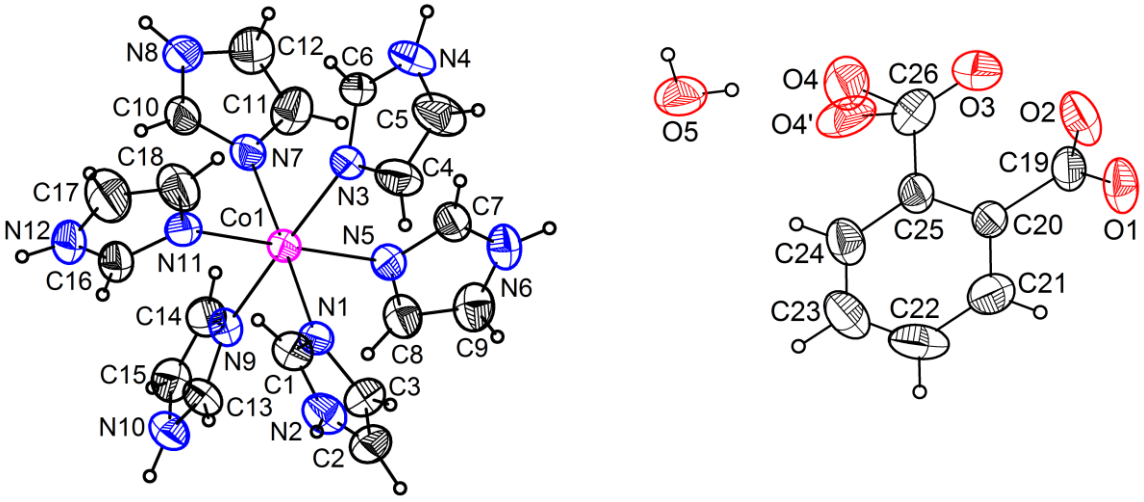

Fig. 8 – The crystal structure of $[Co(Im)_6](pht)\cdot H_2O$ (**5**) showing the atom labelling scheme and the coordination sphere of Co(II) in **5**. Displacement ellipsoids are drawn at the 50% probability level excepting for the H atoms, which are shown as spheres of arbitrary radius

An analysis of the crystal structure reveals the presence of N-H···O, C-H···O and O-H···O H-bonding interactions (Table S5). The $[Co(im)_6]^{2+}$ cation acts as a H-donor via uncoordinated nitrogens of imidazole ligand and the carbon atoms via N-H···O and C-H···O interactions respectively (Fig. S29). On the other hand, phthalate acts as H-acceptor accepting hydrogens from the cation and the lattice water molecule. The lattice water accepts proton from the cation and donates the hydrogens to phthalate anion (Fig. S29). $[Co(im)_6]^{2+}$ cation is H-bonded to six symmetry related phthalate dianions and a lattice water molecule in its surrounding (Fig. S30). The $[Co(im)_6]^{2+}$ unit, phthalate and lattice water molecules are organised in a zig zag fashion in crystallographic *ab* plane (Fig. S31 – S32). An

Published in February 2019 issue of Journal of Molecular Structure
https://doi.org/10.1016/j.molstruc.2018.10.012

O-H···O interaction between phthalate and lattice water leads to a 1-D zig-zag chain along *c-axis* (Fig. 33). H-bonding interactions between cation, anion and lattice water molecule results in 3-D supramolecular architecture (Fig. S34). Unlike in **1-3**, no Cg···Cg distances involving phthalate ring is observed in **4** and **5** which can be explained due to presence of a single unique phthalate in the crystal structure of these 1:1 phthalates. Compound **6** exhibits Cg···Cg distances between the centroids of two unique phthalate rings of the order 4.5 Å and more which are longer than in **1-3** (Table S6).

Conclusions

Using the cyclic diamine piperazine (pip) as a structure directing agent we have accomplished the synthesis of anionic phthalates of general formula $(pipH_2)[M(H_2O)_4(pht)_2]\cdot 8H_2O$ (M= Ni (**1**), Co (**2**), Cu (**3**)). The facile formation of **1**, **2** or **3** under a variety of conditions reveals that when bivalent metal ions, phthalate dianion and piperazinediium cation are present in an aqueous solution, the constituents self assemble to form tetraaqua octahydrates viz. $(pipH_2)[M(pht)_2(H_2O)_4]\cdot 8H_2O$ as the major product. Attempts to exchange the four coordinated water molecules by N-donor ligands afforded the hexaimidazole compounds **4** or **5** or the known dicopper compound **6** all of which exhibit a metal:phthalate ratio of 1:1 and are devoid of any organic cation.

Compounds **1-3** are rare examples of water rich compounds which exhibit a metal:water ratio of 1:12. The crystallographic analysis of **1-3** reveals that the phthalate anion functions as a monodentate ligand and does not exhibit any bridging binding mode. This can be explained to the high degree of hydration of compounds **1-3** which are tetraaqua octahydrates. The lattice water molecules in **1-3** are organised into a water dodecamer cluster with the aid of intramolecular H-bonding to obtain an extended T4(2)6(2) pattern. The importance of the weak secondary interactions in **1-3** can be evidenced by the (Cg···Cg) distances of ~4.0 Å showing π···π stacking of the phthalates. Interestingly such a phthalate stacking is not observed in the hexaimidazole derivatives **4** and **5** which are 1:1 compounds namely neutral metal phthalates. The water rich compounds **1-3** can be fully dehydrated and the anhydrous compounds thus obtained can be rehydrated. During de- and rehydration, compounds **1** and **2** exhibit crystalline-amorphous-crystalline transformation. Our current efforts are directed towards use of piperazinediium cation as charge balancing ion, to obtain similar compounds

Published in February 2019 issue of Journal of Molecular Structure
https://doi.org/10.1016/j.molstruc.2018.10.012

viz. $(pipH_2)[M(pht)_2(H_2O)_4]\cdot 8H_2O$ (M=bivalent metal) by use of other bivalent metals like Mg, Mn, Cd which are known to prefer octahedral geometry.

Supplementary Material

Supplementary data associated with this article can be found, in the online version, at **********. The crystal data were deposited at the Cambridge Crystallographic Data Centre and following CCDC numbers have been assigned 1577837, 1577838, 1577839, 1812302, 1577840, 1812301 for compounds **1-6** respectively. These data can be obtained free of charge via www.ccdc.cam.ac.uk/data_request/cif, or by emailing data_request@ccdc.cam.ac.uk, or by contacting The Cambridge Crystallographic Data Centre, 12, Union Road, Cambridge CB2 1EZ, UK; fax: +44 1223 336033.

Acknowledgements

The authors thank the Sophisticated Analytical Instrument Facility (SAIF), Indian Institute of Technology (IIT) Madras for the single crystal analysis of **2-6** reported in this paper and Dr. P. Raghavaiah from Dr. Harisingh Gour University, Sagar, India for several helpful discussions. We thank one of the reviewers for the (Cg···Cg) distances of **1** in Table 3. This work is supported by University Grants Commission (UGC), New Delhi under the Special Assistance Program. RJ gratefully acknowledges UGC for BSR fellowship.

Published in February 2019 issue of Journal of Molecular Structure
https://doi.org/10.1016/j.molstruc.2018.10.012

References

1) C. Janiak, Dalton Trans. (2003) 2781-2804. http://doi.org/10.1039/B305705B

2) H. Li, M. Eddaoudi, M. O'Keeffe, O.M. Yaghi, Nature 402 (1999) 276-279. https://www.nature.com/articles/46248

3) CSD version 5.38 (2017).

4) R.N. Jyai, B.R. Srinivasan, Indian J. Chem 54A (2015) 1402-1408. http://nopr.niscair.res.in/handle/123456789/33428

5) R. Murugavel, D. Krishnamurthy, M. Sathiyendiran, J. Chem. Soc., Dalton Trans. (2002) 34–39. https://doi.org/10.1039/B105687P

6) K.R. Mote, J. Thomas, A. Ramanan, Indian J. Chem 57A (2018) 1081-1091. http://nopr.niscair.res.in/handle/123456789/44893

7) S.G. Baca, I.G. Filippova, O.A. Gherco, M. Gdaniec, Y.A. Simonov, N.V. Gerbeleu, P. Franz, R. Basler, S. Decurtins, Inorg. Chim. Acta 357 (2004) 3419-3429. https://doi.org/10.1016/S0020-1693(03)00498-5

8) N. Zhao, Y.-E. Deng, P. Liu, C.-X. An, T.-X. Wang, Z.-X. Lian, Polyhedron 85 (2015) 607-614. https://doi.org/10.1016/j.poly.2014.09.021

9) A.D. Burrows, R.W. Harrington, M.F. Mahon, S.J. Teat, Cryst. Growth Des. 4 (2004) 813-822. https://doi.org/10.1021/cg049930a

10) H. Endres, Z. Anorg. Allg. Chem. 513 (1984) 78-88. https://doi.org/10.1002/zaac.19845130609

11) H.-Y. Bai, Y.-Y. Liu, Zeitschrift fur Kristallogr. - NCS 225 (2010) 507-508. https://doi.org/10.1002/zaac.19845130609

12) L. Tian, L. Chen, S.-H. Shen, C.-L. Wen, S. Liu, J. Coord. Chem. 60 (2007) 683-689. https://doi.org/10.1080/00958970600899856

13) H. Küppers, Zeitschrift fur Kristallographie 192 (1990) 97-102. https://doi.org/10.1524/zkri.1990.192.14.97

14) P. Lightfoot, A. J. Snedden, Chem. Soc., Dalton Trans. (1999) 3549-3551. https://doi.org/10.1039/A905726I

15) S. Sengupta, S. Ganguly, A. Goswami, S. Bala, S. Bhattacharya, R. Mondal, CrystEngComm 14 (2012) 7428-7437. https://doi.org/10.1039/c2ce25256b

16) D.K. Kumar, A. Das, P. Dastidar J. Mol. Struct. 796 (2006) 139-145. https://doi.org/10.1016/j.molstruc.2006.02.033

17) L. Tian, L. Chen, X.J Zhang, J. Chem. Crystallogr. 40 (2010) 664-667. https://doi.org/10.1007/s10870-010-9716-8

18) A.L. Pochodylo, K.M. Blake, M.A. Braverman, G.A. Farnum, R.L. LaDuca, Inorg. Chim. Acta 363 (2010) 3951-3958. https://doi.org/10.1016/j.ica.2010.07.061

Published in February 2019 issue of Journal of Molecular Structure
https://doi.org/10.1016/j.molstruc.2018.10.012

19) C.Y. Wang, Z.M. Wilseck, R.M. Supkowskic, R.L. LaDuca, CrystEngComm 13 (2011) 1391-1399. https://doi.org/10.1039/c0ce00632g

20) L.-P. Zhang, J.-F. Ma, J. Yang, Y.-Y. Liu, G.-H. Wei, Cryst. Growth Des. 9 (2009) 4660-4673. https://doi.org/10.1021/cg900460k

21) Y. Wang, F.-H. Zhao, A.-H. Shi, Y.-X. Che, J.-M. Zheng, Y. Wang, F.-H. Zhao, A.-H. Shi, Y.-X. Che, J.-M. Zheng, Inorg. Chem. Commun. 20 (2012) 23-26. https://doi.org/10.1016/j.inoche.2012.02.005

22) S.G. Baca, M.T. Reetz, R. Goddard, I.G. Filippova, Y.A. Simonov, M. Gdaniec, N. Gerbeleu, Polyhedron 25 (2006) 1215-1222. https://doi.org/10.1016/j.poly.2005.09.003

23) G.-F. Hou, B. Wena, Y.-H. Yu, J.-S. Gao, X.-D. Wang, P.-F. Yan, Inorg. Chim. Acta 402 (2013) 128-132. http://doi.org/10.1016/j.ica.2013.03.046

24) L.-N. Zhu, M. Liang, Q.-L. Wang, W.-Z. Wang, D.-Z. Liao, Z.-H. Jiang, S.-P. Yan, P. Cheng, J. Mol. Struct. 657 (2003) 157-163. https://doi.org/10.1016/S0022-2860(03)00365-X

25) S.K. Shakhatreh, E.G. Bakalbassis, I. Brudgam, H. Hartl, J. Mrozinski, C.A. Tsipis, Inorg. Chem. 30 (1991) 2801-2806. https://doi.org/10.1021/ic00013a018

26) H.-X. Zhao, G.-L. Zhuang, S.-T. Wu, L.-S. Long, H.-Y. Guo, Z.-G. Ye, R.-B. Huang, L.-S. Zheng, Chem. Commun. (2009) 1644-1646. https://doi.org/10.1039/b820500k

27) H.-Y. Lin, B. Mu, X.-L. Wang, P. Liu, C. Xu, G.-C. Liu, Z. Anorg. Allg. Chem. 638 (2012) 1504-1511. https://doi.org/10.1002/zaac.201200193

28) A. Kellett, M. O'Connor, M. McCann, M. McNamara, P. Lynch, G. Rosair, V. McKee, B. Creaven, M. Walsh, S. McClean, A. Foltyn, D. O'Shea, O. Howe, M. Devereux, Dalton Trans. 40 (2011) 1024-1027. https://doi.org/10.1039/C0DT01607A

29) Y. Wang, S. Cui, L. Wang, X. Zhang, B. Lia, J. Zhang, CrystEngComm 12 (2010) 2734-2739. https://doi.org/10.1039/b925615f

30) Y. Zhang, J. Lia, Q. Su, Q. Wang, X. Wu, J. Mol. Struct. 516 (2000) 231-236. https://doi.org/10.1016/S0022-2860(99)00203-3

31) M.A. Braverman, J.H. Nettleman, R.M. Supkowski, R.L. LaDuca, Inorg. Chem. 48 (2009) 4918-4926. https://doi.org/10.1021/ic900331m

32) C.D. Nicola, F. Garau, A. Lanza, M. Monari, L. Pandolfo, C. Pettinari, A. Zorzi, Inorg. Chim. Acta 416 (2014) 186-194. http://dx.doi.org/10.1016/j.ica.2014.03.024

33) G.-B. Li, L. Li, J.-M. Liu, T. Yang, C.-Y. Su, Cryst. Growth Des. 13 (2013)1518-1525. https://doi.org/10.1021/cg3017563

34) J. Zdravkovic´, D. Poleti, J. Rogan, D.M. Minic´, Polyhedron 80 (2014) 256-264. http://doi.org/10.1016/j.poly.2014.05.026

35) L.L. Johnston, D.P. Martin, R.M. Supkowski, R.L. LaDuca, Inorg. Chim. Acta 361 (2008) 2887-2894. https://doi.org/10.1016/j.ica.2008.02.040

36) W. Xu, W.-J. Pan, Y.-Q. Zheng, J. Coord. Chem. 66 (2013) 4415-4429. http://doi.org/10.1080/00958972.2013.862789

Published in February 2019 issue of Journal of Molecular Structure
https://doi.org/10.1016/j.molstruc.2018.10.012

37) H.-X. Zhang, B.-S. Kang, A.-W. Xu, Z.-N. Chen, Z.-Y. Zhou, A.S.C. Chan, K.-B. Yu, C. Ren, J. Chem. Soc. Dalton Trans. (2001) 2559-2566. https://doi.org/10.1039/b102570h

38) I.G. Filippova, O.A. Gherco, Y.A. Simonov, A.A. Deseatnic-Ciloci, S.F. Clapco, J.P. Tiurina, S.G. Baca, Polyhedron 29 (2010) 1102-1108. https://doi.org/10.1016/j.poly.2009.11.016

39) X.-C. Fu, X.-Y. Wang, M.-T. Li, C.-G. Wang, X.-T. Deng, Acta Cryst. C62 (2006) m343-m345. https://doi.org/10.1107/S0108270106019068

40) Bruker SMART V5.630, SAINT-PLUS V6.45 and SADABS Bruker-Nonius Analytical X-ray Systems Inc., Madison, Wisconsin, USA, 2003.

41) G.M. Sheldrick, Acta Cryst. A64 (2008) 112-122. https://doi.org/10.1107/S0108767307043930

42) Z.M. Jin, Y.J. Pan, L. He, Z.G. Li, K.B. Yu, Anal. Sci. 19 (2003) 333-334. https://doi.org/10.2116/analsci.19.333

43) R.L. Dutta and A. Shyamal, Elements of magnetochemistry, Second Edition (1993)

44) B.R. Srinivasan, S.N. Dhuri, M. Poisot, C. Näther, W. Bensch, Z Anorg. Allg. Chem. 631 (2005) 1087-1094. https://doi.org/10.1002/zaac.200400513

45) H. Ishira, K. Horiuchi, I. Svoboda, H. Fuess, T. M. Gesing, J. C. Buhl, H. Terao, Z Naturforsch 61b (2006) 69-72. http://www.znaturforsch.com/ab/v61b/s61b0069.pdf

46) Q.-X. Yao, X.-H. Jin, Z.-F. Ju, H.-X. Zhang, J. Zhang, CrystEngComm 11 (2009) 1502-1504. https://doi.org/10.1039/B901516G

47) L. Infantes, J. Chisholm, S. Matherwell, CrystEngComm 5 (2003) 480-486. https://doi.org/10.1039/B312846F

48) J.-H. Wang, G.-M. Tang, Y.-T. Wang, T.-X. Qin, S.W. Ng, CrystEngComm 16 (2014) 2660-2683. https://doi.org/10.1039/C3CE42099J

49) An Introduction to Hydrogen Bonding, ed. G.A. Jeffrey, Oxford University Press, New York, (1997).

50) A.H. Narten, W.E. Thiessen, L. Blum, Sci. 217 (1982) 1033-1034. https://doi.org/10.1126/science.217.4564.1033

51) C.A. Hunter, J.K.M. Sanders, J. Am. Chem. Soc. 112 (1990) 5525-5534. https://doi.org/10.1021/ja00170a016

52) A.L. Spek, Acta Cryst. D65 (2009) 148-155. https://doi.org/10.1107/S090744490804362X

53) R. Kruszynski, T. Sierański, Cryst. Growth Des. 16 (2016) 587−595. https://doi.org/10.1021/acs.cgd.5b00852

Published in February 2019 issue of Journal of Molecular Structure https://doi.org/10.1016/j.molstruc.2018.10.012

Table 1 – Crystal data and structure refinement for **1-6**

	1	**2**	**3**	**4**	**5**	**6**
Empirical formula	$C_{20}H_{44}N_2NiO_{20}$	$C_{20}H_{44}N_2CoO_{20}$	$C_{20}H_{44}N_2CuO_{20}$	$C_{26}H_{30}N_{12}NiO_5$	$C_{26}H_{30}CoN_{12}O_5$	$C_{28}H_{28}Cu_2N_8O_{10}$
Formula weight (g mol^{-1})	691.28	691.5	696.11	649.33	649.55	763.66
Temperature (K)	293(2)	296(2)	296(2)	293(2)	293(2)	296(2)
Wavelength (Å)	1.54184	0.71073	0.71073	0.71073	0.71073	0.71073
Crystal system	Triclinic	Triclinic	Triclinic	Monoclinic	Monoclinic	Monoclinic
Space group	*Pī*	*Pī*	*Pī*	$P2_1/c$	$P2_1/c$	$P2_1/n$
Unit cell dimensions						
a (Å)	11.2600(6)	11.8572(3)	11.9101(5)	13.0759(6)	13.1134(4)	8.8768(4)
b (Å)	11.8393(7)	12.4961(3)	12.3555(6)	13.0309(7)	13.0374(4)	22.3595(12)
c (Å)	12.4959(7)	27.2165(6)	16.6034(7)	18.4208(9)	18.4269(6)	16.1084(9)
α (°)	82.000(5)	79.0500(10)	100.649(2)	90	90	90
β (°)	77.409(5)	88.6480(10)	97.357(2)	105.636(2)	105.388(2)	105. 454 (2)
γ (°)	75.538(5)	82.0290(10)	96.264(2)	90	90	90
Volume (Å^3)	1567.92(15)	3920.95(16)	2359.23(18)	3022.6(3)	3037.41(17)	3081.6(3)
Z	2	5	3	4	4	4
D_{calc} (mg/m^3)	1.464	1.464	1.4703	1.427	1.420	1.646
Absorption coefficient (mm^{-1})	1.660	0.632	0.779	0.699	0.622	1.451
F(000)	732	1825	1101	1352	1348	1560
Crystal size (mm^3)	0.37 x 0.27 x 0.26	0.30 x 0.25 x 0.20	0.25 x 0.20 x 0.20	0.40 x 0.30 x 0.30	0.40 x 0.30 x 0.30	0.30 x 0.30 x 0.25
θ range for data collection (°)	3.64 to 67.08	1.70 to 25.00	1.90 to 25.00	2.25 to 25.00	2.244 to 25.00	2.245 to 26.999
Index ranges	$-9 \le h \le 13$	$-14 \le h \le 14$	$-14 \le h \le 14$	$-15 \le h \le 15$	$-15 \le h \le 15$	$-11 \le h \le 11$
	$-14 \le k \le 14$	$-14 \le k \le 14$	$-14 \le k \le 14$	$-15 \le k \le 15$	$-15 \le k \le 15$	$-28 \le k \le 28$
	$-14 \le l \le 14$	$-32 \le l \le 32$	$-19 \le l \le 19$	$-21 \le l \le 21$	$-21 \le l \le 21$	$-20 \le l \le 20$
Reflections collected / unique	9530 / 5572	97359 / 13783	61059 / 8318	51915 / 5305	45501 / 5337	51507 / 6736
	[R(int) = 0.0166]	[R(int) = 0.0371]	[R(int) = 0.0383]	[R(int) = 0.0428]	[R(int) = 0.0386]	[R(int) = 0.0308]
Completeness to θ (°)	99.8% (67.08)	99.9% (25.00)	99.9% (25.00)	99.8% (25.00)	100% (25.00)	100% (25.00)
Absorption correction	Multi-scan			Full-matrix least-squares on F^2 for **1-5**		
Refinement method			Semi-empirical from equivalents for all compounds			
Max. and min. Transmission	0.6721 and 0.5787	0.8840 and 0.8330	0.8598 and 0.8291	0.90 and 0.75	0.8353 and 0.7889	0.73 and 0.55
Data / restraints / parameters	5572/ 1 /447	13783 / 99 / 1151	8318 / 54 / 714	5305 / 3 / 405	5337 / 10 / 416	6736 / 15 / 449
Goodness-of-fit on F^2	1.037	1.052	1.054	1.082	1.146	1.045
Final R indices [I>2sigma(I)]	R1 = 0.0351,	R1 = 0.0311,	R1 = 0.0290,	R1 = 0.0398,	R1 = 0.0376,	R1 = 0.0298,
	wR2 = 0.0993	wR2 = 0.0850	wR2 = 0.0755	wR2 = 0.1053	wR2 = 0.0820	wR2 = 0.0683
R indices (all data)	R1 = 0.0366,	R1 = 0.0515,	R1 = 0.0474,	R1 = 0.0625,	R1 = 0.0583,	R1 = 0.0407,
	wR2 = 0.1009	wR2 = 0.1001	wR2 = 0.0876	wR2 = 0.1295	wR2 = 0.1009	wR2 = 0.0732
Largest diff. peak and hole (e Å^{-3})	0.374 and -0.415	0.406 and -0.442	0.286 and -0.467	0.464 and -0.430	0.368 and -0.374	0.416 and -0.308